Segmental Relaxation And Partial Crystallization Of Chain-Extended Poly(L-Lactic Acid) Reinforced With Carboxylated Carbon Nanotube

Omid Yousefzade[a,c,§], Sofia Valenti[b,c,§], Jordi Puiggali[c,*], Hamid Garmabi[a], Roberto Macovez[b,*]

[a]Department of Polymer Engineering and Color Technology, Amirkabir University of Technology, Tehran, Iran

[b]Department de Física and Barcelona Research Center in Multiscale Science and Engineering, Universitat Politècnica de Catalunya, Escola d'Enginyeria de Barcelona Est-EEBE, c/Eduard Maristany 10-14, Barcelona E-08019, Spain

[c]Chemical Engineering Department and Barcelona Research Center in Multiscale Science and Engineering, Universitat Politècnica de Catalunya, Escola d'Enginyeria de Barcelona Est-EEBE, c/Eduard Maristany 10-14, Barcelona E-08019, Spain

§ These two authors contributed equally

Email addresses:

Jordi.Puiggali@upc.edu

roberto.macovez@upc.edu

*Authors to whom correspondence may be addressed.

ABSTRACT

Temperature-modulated differential scanning calorimetry (TMDSC) and broadband dielectric spectroscopy (BDS) were employed to study the glass transition, size of the cooperative rearranging regions (CRR), crystallization kinetics and dielectric relaxation response of nanocomposites constituted by chain-extended poly(L-lactide) (PLLA) and carboxylated carbon nanotubes (f-CNTs). The CRR size and the number of relaxing structural units decreased in the presence of crystals during isothermal crystallization. All samples displayed both a primary (α) and secondary (β) relaxation in BDS spectra. The relaxation dynamics of PLLA chains was barely affected by the presence of the f-CNT. Constrained polymer chains and thickness of interphase (t_i) were measured using dielectric spectra in tan δ representation. t_i values were found to be 46 and 24 nm for sample containing 0.2 and 0.5 percent weight fraction of f-CNT, respectively. All samples underwent partial crystallization (with roughly 30% of final crystalline fraction) some 15 or 20 degrees above their T_g. Crystallization leads to a fragile-to-strong transition in the temperature dependence of the cooperative α relaxation, and to the increased visibility of a Maxwell-Wagner-Sillars interfacial relaxation which appears to be present in all samples. The heterogeneity of the polymeric samples was quantified in terms of a new parameter, the heterogeneity index (*H*).

Keywords: PLLA nanocomposites, cooperative rearranging region, chain dynamics, heterogeneity, constrained polymer chains.

INTRODUCTION

Understanding the dynamics of polymer chains in the viscoelastic state is an important prerequisite to design and modify the final properties of polymers (i.e. mechanical properties)[1-3]. Measurement of the temperature dependence of the relaxation time provides insight on the variation of polymer chain dynamics in the presence of additives and/or modifiers [4-6], and can be used to define a "dynamic" glass transition temperature of the system. The effect of sample heterogeneity and of the ensuing dynamical heterogeneity on the glass transition has attracted increasing attention recently [7]. The concept of cooperative rearranging region (CRR) was introduced by Adam and Gibbs to characterize the dynamics of polymer chains at and above the glass transition temperature (T_g) [8]. A CRR is defined as a subsystem which can rearrange its configuration independently of its environment. According to the method developed by Donth et al., [9-11] the size of the CRR can be determined by a spatial criterion based on the statistical independence of thermal fluctuations. These in turn can be calculated from the measurement of the complex heat capacity using temperature modulated differential scanning calorimetry (TMDSC). The cooperativity length at the glass transition, ξ_a, can be easily estimated using the temperature fluctuation of the amorphous phase. The cooperativity length ξ_a associated with the volume of a CRR, $V_a = \xi_a^3$ and the number of relaxing structural units per CRR, N_a (i.e. the also called the cooperativity degree) can be estimated by [10]:

$$V_a = \xi_a^3 = \frac{\Delta C_p^{-1} k_B T_\alpha^2}{\rho(\delta T)^2} \quad (1)$$

$$N_a = \frac{N_A k_B T_a^2 \Delta C_p^{-1}}{m_0 (\delta T)^2} \quad (2)$$

Where T_α is the dynamic (calorimetric) glass transition temperature, ΔC_p^{-1} is the difference in the inverse of the isobaric heat capacity between the liquid and the glass at T_α, ρ is the density

at T_α, k_B is the Boltzmann constant, N_A is Avogadro's number, m_0 is the molar mass of the relaxing structural unit and δT is the temperature fluctuation in a CRR. One usually assumes that the mean temperature fluctuation, δT, is associated to the standard deviation of the dissipation peak $C''(T)$ (fitted assuming a Gaussian line shape), which was obtained by means of temperature-modulated differential scanning calorimetry (TMDSC).

It was found that the molecular weight of the polymer, the presence of crystalline regions, and that of nanoparticles dispersed in the polymer matrix, are all factors that influence the size of CRR [12-14]. This is because the characteristic CRR size of amorphous polymers is in the range of a few nm, which is also the typical range of polymer-filler interaction.

Polymer-nanoparticle interactions in polymer nanocomposites have been widely investigated in recent years. Many studies focus on the determination of glass transition parameters by means of differential scanning calorimetry (DSC) [15], and of the segmental relaxation times by techniques such as broadband dielectric spectroscopy (BDS) [16] and dynamic mechanical analysis (DMA) [17]. Application of these techniques also allows estimating the thickness of interphase between polymer and nanoparticles [18, 19]. The segmental relaxation of the polymer turns out to be quite different in the vicinity of the nanoparticles than in the bulk of the amorphous polymer matrix [20, 21]. The experimental results may be straightforwardly interpreted in terms of models that take into account the fraction of interfacial polymer, and allow determining the thickness of the interfacial layer [19, 22].

Dielectric spectroscopy is a versatile tool that provides useful information on the intensity (dielectric strength) and relaxation time of the macromolecular dynamic processes [23, 24]. In addition, the dielectric analysis of heterogeneous materials allows studying interfacial effects such as Maxwell-Wagner–Sillars (MWS) relaxations [25]. The origin of the MWS relaxation is the formation of interfacial dipoles arising from the accumulation of bound and/or free charges

at the boundary between two media of different conductivity and permittivity, leading to the appearance of an interfacial polarization [26].

Recently, a new parameter named heterogeneity index was introduced based on the analysis of rheological Cole-Cole plots in the melt state [12]. With this parameter, the impact on sample homogeneity due to the presence of nanoparticles or to the process of chain extension of polymer can be assessed.

In this study, we explore the relaxation dynamics, crystallization kinetics, and heterogeneity effects of chain-extended polylactic acid (PLLA) samples reinforced with carboxylated carbon nanotubes (f-CNTs). The effect of chain extension, crystallinity and amount of f-CNT on the CRR size was studied by conventional scanning calorimetry measurements (DSC) as well as by temperature-modulated calorimetry experiments (TMDSC) in the glass transition temperature range. We also employed BDS in the viscoelastic and semicrystalline states to determine the temperature-dependent dielectric strength and relaxation time of the cooperative segmental relaxation of the polymer. We use the loss tangent (tan(δ)) dielectric spectra to obtain the thickness of interphase, and compare it with the value obtained by a similar method based on dynamical mechanical analysis spectra of amorphous samples.

To the best of our knowledge, this is the first time that BDS is measured on chain-extended PLLA and its nanocomposites. Compared with commercial PLLA samples, our materials show a strong tendency to crystallize above T_g, and they display an interfacial relaxation (of the Maxwell-Wagner-Sillars type) that was not observed previously in PLLA samples, and which we ascribe to heterogeneities such as the chain-extender-polymer and CNT-polymer interfaces. The occurrence of crystallization enables comparison of amorphous and semicrystalline samples and thus allows comparing the CRR size and heterogeneity effects between the two.

EXPERIMENTAL SECTION

Materials

Poly (L-lactide) (PLLA), grade 4032D, was purchased from Natureworks LLC, USA. It is a semi-crystalline material containing 2% of D-lactide units. Multiwalled carbon nanotubes (with average diameter, length and specific surface area of 9.5 nm, 1.5 μm and 250–300 m^2 g^{-1}, respectively) were provided by Nanocyl (Nanocyl7000 series, Belgium). Commercial multifunctional styrene-acrylic oligomers (BASF, Joncryl® ADR-4368) were used as a reactive agent.

Sample Preparation

Carboxylated CNTs were first prepared through acid oxidation process developed in our previous work [27]. Subsequently, the PLLA/CNTs master batch with 5 wt-% MWCNTs was prepared using solution casting. In order to get nanocomposites with different MWCNT loadings, the obtained masterbatch was melt compounded with the appropriate amounts of PLLA in the presence or absence of the selected chain modifier (i.e. Joncryl® ADR) for reactive and non-reactive melt mixing, respectively. A lab-scale internal mixer (Brabender mixer, PL2200) was employed, being the operating conditions 190 ºC for temperature and a rotor speed of 60 rpm. Chain extender reactions were considered to be completed when a plateau in torque curves was achieved. This time was 15 min for the longest case and therefore was applied for all studied samples including those prepared without Joncryl® and MWCNTs. The amount of this chain modifier was set to 0.5 *wt*-% for all samples prepared via reactive melt mixing. The studied samples are named by the abbreviation PLA/f-CNTx/Y. The number after CNT shows its weight fraction in the nanocomposite and the upper case at the end of the code indicates reactive (R) or non-reactive (N) melt mixing, e.g. PLA/f-CNT0.5/R corresponds to the nanocomposite containing 0.5 *wt*-% of carboxylated MWCNTs prepared by reactive melt mixing, whereas

PLA/f-CNT0.2/N corresponds to the nanocomposite containing 0.2 *wt*-% of carboxylated MWCNTs during non-reactive melt mixing. The dispersion state of MWCNTs in the PLLA matrix and the effect of chain extension process on the molecular weight and structure of PLLA were discussed in our previous work [12, 27].

Characterization

Transmission electron microscopy (TEM) characterization was carried out by means of a Philips TECNAI 10 microscope operating at 80 kV and employed to evaluate the morphology and dispersion of CNT in the prepared nanocomposites.

The TMDSC analysis was performed on a TA Instrument DSC Q100. Samples with 4-5 mg mass, initially either fully amorphous or semicrystalline, were encapsulated in aluminum pans. Amorphous samples were obtained by a fast cooling (i.e. at the maximum rate allowed by the equipment) from the melt state to room temperature. Semicrystalline samples were obtained by allowing isothermal crystallization at 130 ºC. Experiments were performed in a nitrogen atmosphere and a flow rate of 50 mL/min. The modulated temperature program corresponded to a sinusoidal temperature profile with a heating rate of 2 ºC/min, amplitude of 0.32 ºC and a modulation period of 60 s in the range of 25-75 °C. Sample heat capacities at different temperature were determined to evaluate the cooperativity rearranging region.

Standard DSC was employed to determine the isothermal crystallization kinetics of chain-extended PLLA in the presence or absence of filler. Isothermal crystallizations data were acquired at two different temperatures (80 and 85°C). To this aim, the samples (PLLA/f-CNT0/R and PLLA/f-CNT0.2/R) were first heated to 200 °C (thermal history were erased by keeping the sample in the melt state for two minutes) and then rapidly cooled to room temperature (i.e., to well below the glass transition temperature of PLLA) to avoid crystallization during cooling. The samples were then rapidly heated to the selected isothermal crystallization temperature while constantly acquiring heat flow. The temperatures of 80 or 85 °C were selected for the

crystallization kinetics study because in our temperature-dependent BDS experiments crystallization was observed to take place already at temperatures only 10 or 15 degrees higher than the glass transition temperature of the samples (see Subsection Broad Band Dielectric Spectroscopy Results). The crystallization process at the selected temperatures stopped after a maximum of 120 min, yielding a semicrystalline sample. The amount of crystallinity (*X*) was measured by heating the semicrystalline samples, after the end of the crystallization process, to above their melting point. The values of *X* obtained by $X = \frac{\Delta H_m}{\Delta H_{100\%}}$ where ΔH_m and $\Delta H_{100\%}$ are respectively the melting enthalpy of the samples and the theoretical enthalpy for a 100% crystalline PLLA, which is 93 J/g [28].

A Novocontrol Alpha Analyzer (Novocontrol Technologies GmbH & Co., Germany) was used for broadband dielectric spectroscopy (BDS) measurements. The amorphous sample was placed between two stainless steels electrodes with a diameter of 21 mm. The thickness of the sample (which was of the order of 100 μm in all cases) was measured and used to calculate the empty cell capacity. Temperature control of the capacitor and thus of the sample was achieved with a nitrogen-gas flow cryostat. The temperature was stabilized before each isothermal measurement and the experimental error was not higher than 0.3 K. Isothermal spectra were acquired every 20 K in the range between 150 K and 330 K, and every 1K in the range between 330 K and 370 K. All measurements were done in the frequency (ν) range between 10^{-1} Hz and 10^6 Hz. The results of BDS measurements were analyzed in terms of time scale, relaxation strength and shape of the segmental α relaxation by fitting the Havriliak-Negami (HN) model function to experimental data [29]:

$$\varepsilon^*(f) = \varepsilon_\infty + \frac{\Delta\varepsilon}{(1+(if/f_0)^{\alpha_{HN}})^{\beta_{HN}}} \quad (3)$$

In this equation, f_0 is a characteristic frequency related to the frequency of maximum loss (ε''), ε_∞ describes the value of the real part of dielectric permittivity, ε', for $f>>f_0$, $\Delta\varepsilon$ is the dielectric strength, and α_{HN} and β_{HN} are parameters of the shape of the relaxation.

RESULTS AND DISCUSSION

Size Of Cooperative Rearranging Region And Isothermal Crystallization

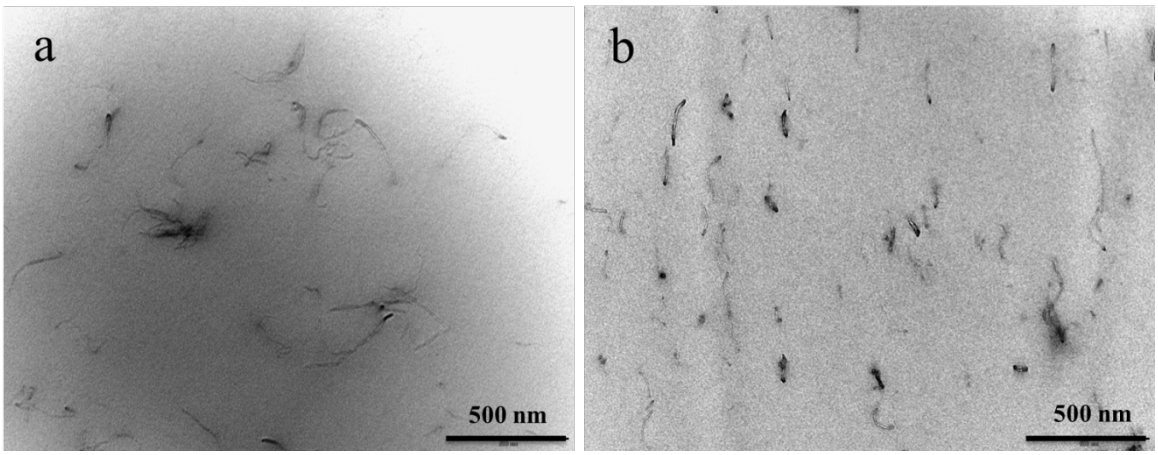

Figure 1. TEM micrographs of PLLA /f-CNT0.2/N (a) and PLLA /f-CNT0.2/R (b)

Before carrying out the DSC and BDS experiments, the morphology of the nanocomposites was characterized by TEM. A homogenous dispersion of carboxylated CNTs in PLLA was observed, whereas aggregation of the nanotubes resulted if non-functionalized CNTs are employed [27]. Figure 1 displays TEM micrographs of both PLLA/CNT (panel a) and chain-extended PLLA/CNT (panel b) nanocomposites. A more homogeneous dispersion state of the CNTs can be observed in the chain-extended PLLA/CNT samples. This shows that bonding between PLLA and CNT during reactive melt mixing resulted in no aggregation of CNT in this sample.

The spatial extent of the cooperative dynamics of the polymer chains at temperatures close to the glass transition can be evaluated by measuring the cooperativity length ξ_a and the number of relaxing structural units per CRR N_a (see equations 1 and 2). The average CRR sizes are

calculated by taking ρ = 1.21 g/cm^3 at 60 ºC, M_0 = 72 g/mol for the unit repeat of PLLA and a temperature fluctuation δT determined as the half-width at half-height of the out of phase C_p spectrum (C"(T)). An example of how to calculate the required physical quantities was shown in a previous paper [12]. Figure 2 shows the out-of-phase (C") and in-phase (C') heat capacities obtained from TMDSC experiments on amorphous and semicrystalline PLLA. Significant differences between the amorphous and semicrystalline samples are obvious in both C' and C" curves. The cooperativity lengths for amorphous and semicrystalline PLLA and the nanocomposites are summarized in Table 1. The size of cooperativity ξ_a and the number of relaxing structural units per CRR, N_a, were found to be smaller in semicrystalline samples obtained by crystallization at 130 °C from the melt.

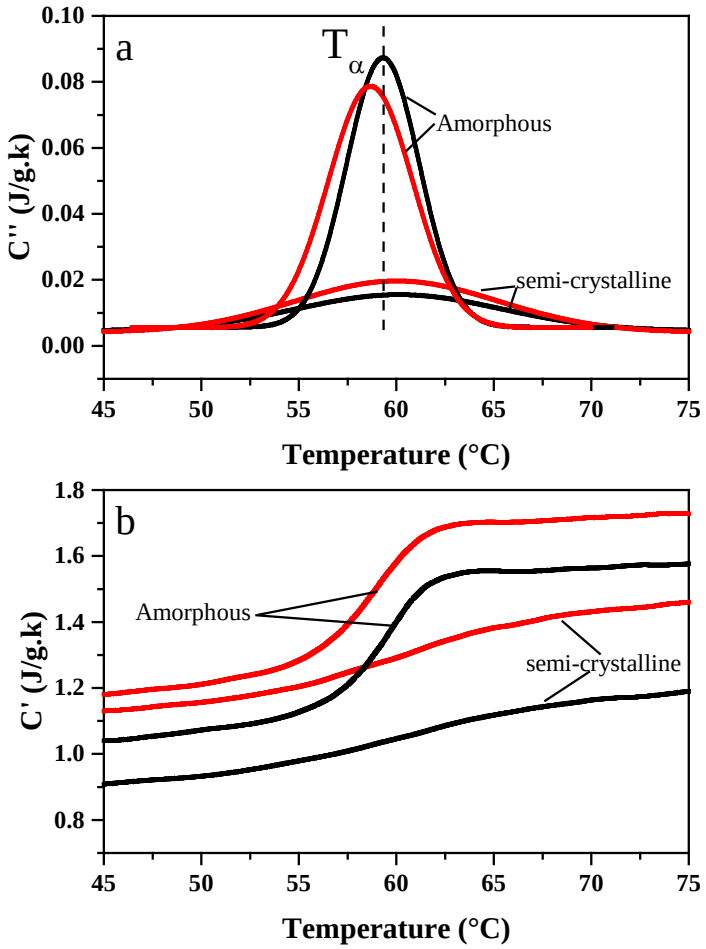

Figure 2. *C*" (a) and *C*' (b) calorimetric response of PLLA/CNT0/N (black lines) and PLLA/CNT0/R (red lines) for amorphous and semicrystalline samples.

According to Table 1, the size of CRR was not significantly influenced by MWCNTs for the amorphous samples. In semicrystalline samples, it seems therefore that it is the presence of crystalline polymer domains that mainly determines the relaxation of polymer chains in the amorphous domains and their typical size and number of relaxing unit, rather than the carbon nanotubes. It was found that the crystallinity increased by addition of MWCNTs in PLLA in isothermal crystallization process at 130 °C (data not shown here). These excess crystals increases the amount of rigid amorphous phase (RAF) resulted in decreasing the size of CRR and also the number of relaxing unit. In amorphous samples, the N_a decreased from 335 to 285 with addition

of f-CNT however the influence of crystallization is much more than f-CNTs. In the rest of the paper we focus on the relaxation dynamics of amorphous and semicrystalline samples, of which three representative ones were selected to study the effect of MWCNTs on the dynamic segmental relaxation of PLLA, namely PLLA/f-CNT0/R, PLLA/f-CNT0.2/R and PLLA/f-CNT0.5/R. For all these, we study the crystallization kinetics and the effect of partial crystallization on the dielectric response.

Table 1. TMDSC data for amorphous and semicrystalline PLLA and its nanocomposites.

Sample	Amorphous (A) or Semicrystalline (S)	T_α (K)	ΔC_p^{-1} (J^{-1}.g.K)	δT (K)	ξ_a (nm)	N_a
PLLA/f-CNT0/N	A	332.4	0.363	3.5	3.4	390
	S	333.2	0.242	6.7	1.9	71
PLLA /f-CNT0.2/N	A	332.4	0.335	3.4	3.3	382
	S	333.2	0.187	7.1	1.7	49
PLLA /f-CNT0/R	A	331.8	0.331	3.6	3.3	335
	S	333.1	0.147	6.1	1.8	52
PLLA /f-CNT0.2/R	A	331.7	0.348	4.0	3.1	285
	S	333.5	0.270	6.0	2.1	99
PLLA /f-CNT0.5/R	A	332.5	0.392	4.2	3.1	292
	S	334.2	0.211	5.7	2.1	86

To study the phase behavior of our samples, isothermal crystallization experiments on amorphous PLLA were performed with DSC. Results of DSC experiments carried out on two samples (PLLA/f-CNT0/R and PLLA/f-CNT0.2/R) at 85°C are shown in Figure 3 in terms of relative degree of crystallinity and corresponding Avrami plot. It is obvious in Figure 3(a) that the kinetic of crystallization for neat PLLA is slower than for PLLA reinforced with MWCNTs. After crystallization came to a halt, the samples were heated again to measure the value of crystallinity. PLLA reinforced with MWCNTs showed slightly higher final crystal fraction, with

both values lying close to 30%. The same experiments were performed at 80 °C and the same trend and final crystalline fraction were observed (not shown).The isothermal crystallization kinetics was investigated by evaluating the degree of crystallinity as a function of time at a constant temperature. The relative crystallinity ($X(t)$) for various crystallization times was calculated from the ratio of the area of the exothermic peak up to a time t divided by the area of the total exotherm. The relative crystallinity as a function of crystallization time was calculated using:

$$X(t) = \frac{\int_0^t (\frac{dH}{dt})dt}{\int_0^\infty (\frac{dH}{dt})dt}$$

where $\frac{dH}{dt}$ is the rate of heat evolution and t is the relative crystallization time.

The theory of Avrami was applied to analyze the isothermal crystallization kinetics of PLLA in the presence of MWCNTs or without filler. To this end the following equations were employed [30]:

$$X(t) = 1 - \exp(-Z t^n) \quad (5)$$

$$\ln[-\ln(1-X(t))] = \ln Z + n \ln t \quad (6)$$

$$k = (Z)^{1/n} \quad (7)$$

$$\tau_{1/2} = (\ln 2)^{1/2}/k \quad (8)$$

where n is the Avrami exponent, which depends on the nucleation mechanism and the crystal growth geometry, $\tau_{1/2}$ is the crystallization half time, and k is the overall crystallization rate constant, which contrary to Z has the correct units of s^{-1} and is related to $\tau_{1/2}$ without the involvement of the exponent n (compare eq. 7 and 8).

The values of n and Z can be obtained from the slope and the intercept in the origin of ln [–ln (1 – $X(t)$)] versus ln (t) plots, respectively. As visible also directly in Figure 3(b), the calculated values of n are the same in both neat PLLA and PLLA with MWCNTs (a small difference comparable with experimental error is observed). Instead, the value of k, which is proportional to the overall crystallization rate, increased from 0.039 min^{-1} to 0.116 min^{-1} with the addition of MWCNTs. In other words, addition of MWCNTs in PLLA increased the overall crystallization rate significantly in these isothermal temperature ranges (about 20 K above the glass transition temperature), but it did not affect much the melting point nor the degree of crystallinity of the samples, as shown in figure S1 of the Supplementary Material. It is interesting to note that the (partial) crystallization of our chain-extended PLLA samples occurred already around 70 or 80º, depending on the crystallization conditions, that is, 10 or 20 degrees above T_g. These temperatures are significantly lower than the crystallization temperature of commercial PLLA. This difference may be related to the presence of the oligomeric chain extender, which is present in the final sample as a short block of a block-copolymer mainly composed of PLLA, and which might favor heterogeneous nucleation of the PLLA crystals.

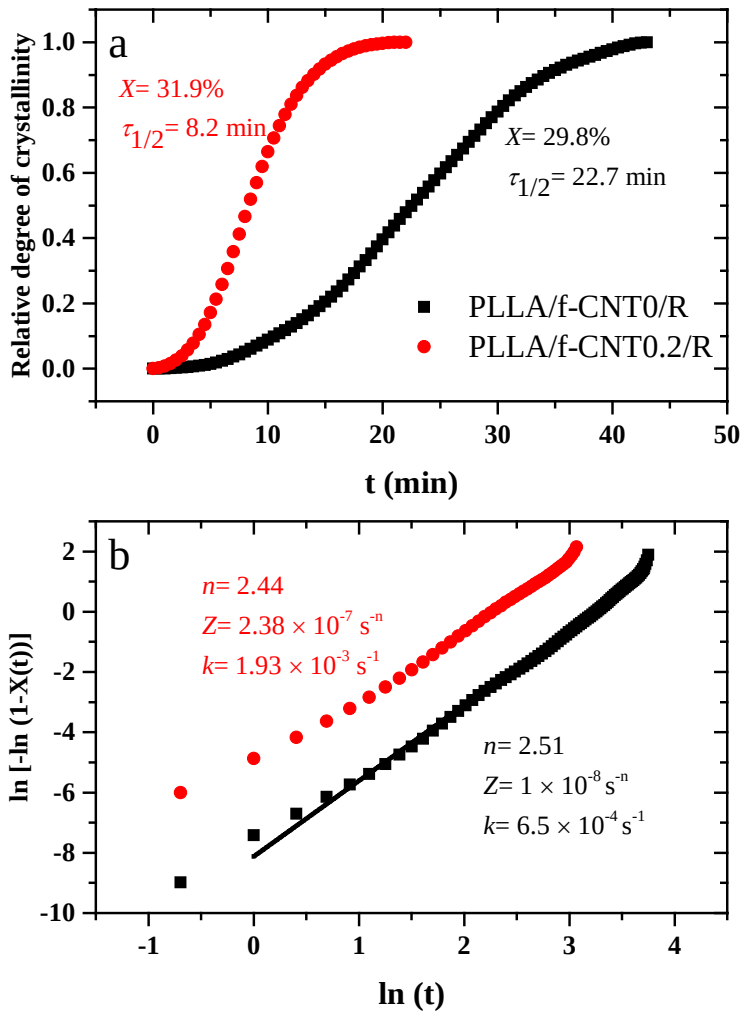

Figure 3. Relative degree of crystallinity vs. time (a) and Avrami plots (b) for the isothermal crystallization at 85 ºC of PLLA/CNT0/R (black lines), PLLA/f-CNT0.2R (red lines).

Broad Band Dielectric Spectroscopy Results

Isothermal BDS measurements were performed on initially amorphous samples at selected temperatures reached by heating up the samples from well below their glass transition temperature (T_g), to study both secondary and primary (segmental) relaxation dynamics. Based on the results presented in the previous Section, above T_g we expect to observe the effect of crystallization of PLLA on the cooperative segmental relaxation. Figure 4 shows representative frequency-dependent spectra of the dielectric loss ε" (a) and dielectric constant ε' (b) of

amorphous PLLA with 0.5 wt.% of functionalized CNT (PLLA/f-CNT0.5/R) prepared via reactive melt mixing. As expected, the spectral features of both ε"' and ε' curves shift to higher frequency with increasing temperature, due to the increased thermal energy that facilitates the movement of polymer chains. As shown in Figure 5, both the tan(δ) spectra as function of frequency, and the Cole-Cole plots, similarly reflect the variation of chain relaxation frequency with increasing temperature. It is interesting to note that the shape and size of the Cole-Cole plots varied significantly with temperature.

The most intense peak in the top panels of Figures 4 and 5 correspond to the cooperative segmental relaxation mode (α relaxation) of the polymer, which is associated with its glass transition. At lower frequency than the α relaxation peak, at about 10^{-1} Hz, another loss feature is observed, which is rather narrow and barely affected by changes in temperature. The occurrence of a relatively narrow relaxation feature that is slower (has a lower frequency) than the α relaxation is typical of heterogeneous samples with internal interfaces and non-negligible conductivity; examples of this dielectric response are the electrode polarization effect and the so-called Maxwell-Wagner-Sillars (MWS) interfacial relaxation, which arises in mixed-phase samples [31] due to the interfacial polarization build-up at phase boundaries. Besides these two features, a much less intense secondary (β) relaxation was observed at lower temperature (few representative temperatures are displayed in both Figures 3 and 4). Both primary and secondary relaxations of PLLA were observed in previous BDS studies [4, 5, 32]. Instead, we did not find any clear spectroscopic evidence for the presence of a normal mode shifting to higher frequency with increasing, contrary to previous reports on pristine PLLA (without chain extension).[5, 33]

It may be observed in all representations of the dielectric spectra, but especially in the permittivity and tan(δ) representations (Figure 4(a,b) and Figure 5(a)), that the intensity of the cooperative α relaxation decreases rather abruptly between 339 and 343 K. The decrease of

dielectric intensity is visible both as a decrease in the height of the loss feature (Figure 4(a)) and as a decrease of the static (low-frequency) value of the real permittivity (dielectric constant, Figure 4(b)). We verified, in a separate experiment (not shown) in which we measured while lowering the sample temperature after acquiring the series of spectra displayed in Figure 4, that the decrease in intensity upon heating was irreversible. Such a behavior is typical of crystallization of supercooled liquids, [34, 35] which in the case of polymers results in only partial crystallization. The fact that our samples crystallize just above T_g rationalizes the lack of observation of the normal mode, which is in fact not detected in semicrystalline commercial PLLA [32].

To visualize more directly the effect of the (partial) crystallization, the inset to Figure 4(b) shows the dielectric strength as extracted from the fit of the permittivity data (see Section 2.3). The ratio of the fitted dielectric strength before and after partial crystallization would indicate that the crystalline polymer fraction is about 50%, which is higher than the crystallinity measured by isothermal DSC experiments (roughly 30%). The discrepancy might be due to the fact that isothermal crystallization in DSC is carried out at 80, 85 ºC or 130 ºC, while crystallization during BDS measurements is observed to take place between 65 and 72 ºC. Crystallization at lower temperature occurs more slowly, and it can lead to a larger size of crystalline domains (spherulites) and favor a higher crystalline fraction. Other differences that might rationalize the observed difference are that the DSC crystallization takes place under isothermal conditions, which is not the case for BDS experiments (the temperature is raised between one spectrum and the next), and that the parallel-plate capacitor geometry is very different from that of DSC experiments.

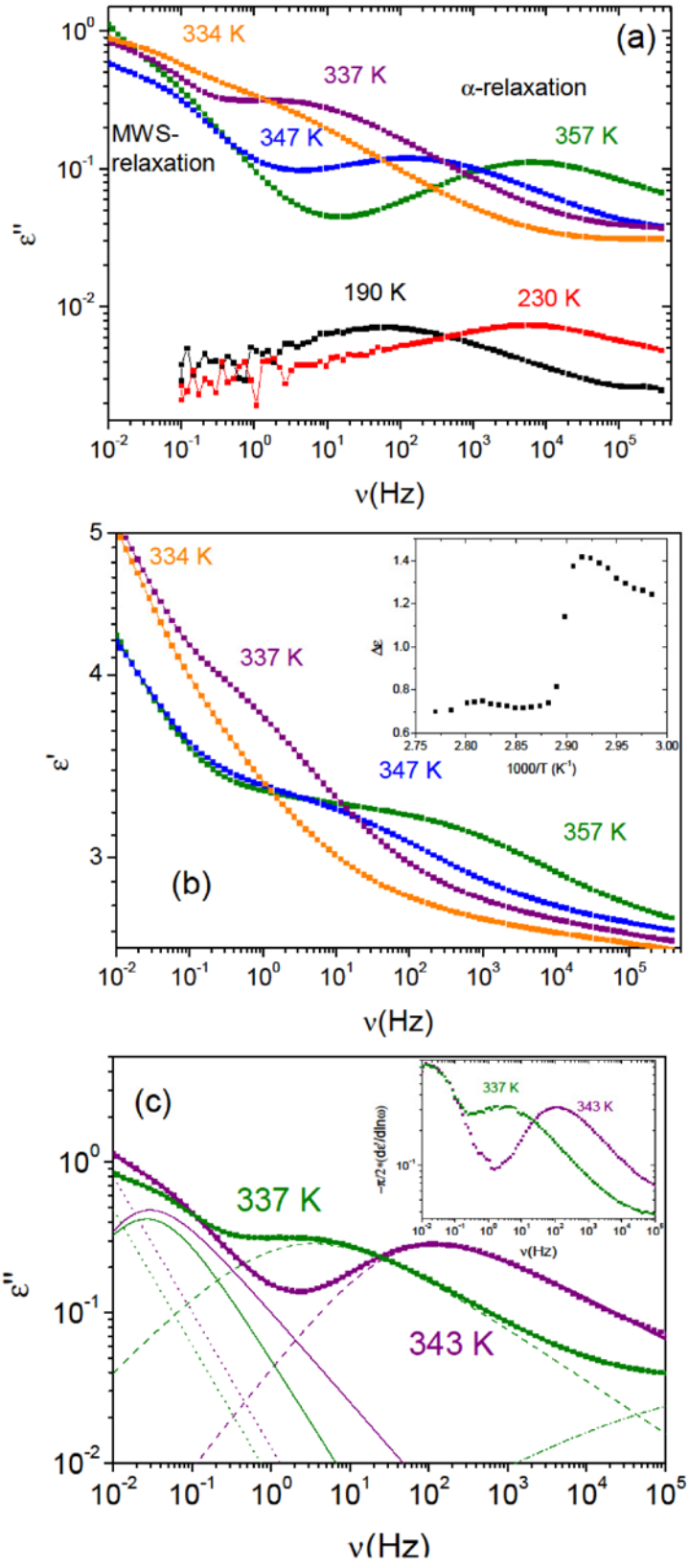

Figure 4. (a,b) Frequency dependent spectra of the dielectric loss (a) and of the dielectric constant (b) for PLLA/f-CNT0.5/R. The spectra are shown in the temperature range between

334 and 357 K, where the segmental mode (α relaxation) is observed, and at lower temperatures (190 and 230 K) where the β relaxation is observed. Inset to panel (b): dielectric strength of the segmental α relaxation as a function of temperature above T_g. (c,d) Frequency dependent spectra of the dielectric loss (symbols) with the contribution of the different relaxations (lines) (c) and derivative of the real part of the dielectric permittivity (d) at two selected temperatures.

The interfacial relaxation at 10^{-1} Hz is observed also before the onset of crystallization, and also in the chain-extended polymer without filler, which shows that it is either intrinsic to the chain-extended polymer sample, or else due to an interfacial effect at the electrode surfaces. To better visualize the presence of this relaxation feature, in Figure 4(c) we show the fit components for two selected temperatures. In the inset to panel (c), we show the derivative of the ε' data [36], which can be considered as an approximate loss spectrum without the conductivity background[37]. In both Figure 4(c) and in its inset, it is clear that the interfacial relaxation is almost invariant with temperature. This rules out an electrode polarization effect, since the latter is due to accumulation of free charge at the electrode-polymer interface and follows the same trend as the conductivity of the sample, which changes with temperature.

We thus associate the observed narrow relaxation to the occurrence of an interfacial polarization between internal regions of different permittivity and conductivity (MWS relaxation). Since this relaxation is not visible in pristine PLLA (it was in fact never reported in previous studies), but it is visible in our chain-extended samples we ascribe it to a boundary effect due to the fact that our chain-extended PLLA samples are actually block copolymers with an intrinsic heterogeneity. The lack of temperature dependence suggests either that the relaxation time only depends on static permittivity values, which barely change for T above the glass transition temperature and which are a priori different for PLLA and the chain extender,

or that the conductivity of one of the interfacial regions is much larger than that of the other. This latter could be the case for the polymer-CNT interface, for example, where the interfacial relaxation is more visible.

The crystallization of the polymer component above T_g observed in Figure 4 does not result in a shift in frequency of the interfacial relaxation. Upon crystallization, not only the intensity of the α relaxation decreases, but also the low-frequency conductivity background (Figure 4(a)) and the intensity of the MWS relaxation appear to do so. As discussed in the following, the pure polymer samples displayed a behavior very similar to that of the nanocomposite samples. The intensity of the MWS relaxation was higher in the nanocomposites than in the pure sample, which we take as an indication of a higher heterogeneity of the samples with the nanofillers. The heterogeneity in the system also results in the appearance of a tail in the Cole-Cole plots (Figure 5(b)), corresponding to the spectral region of the MWS interfacial relaxation.

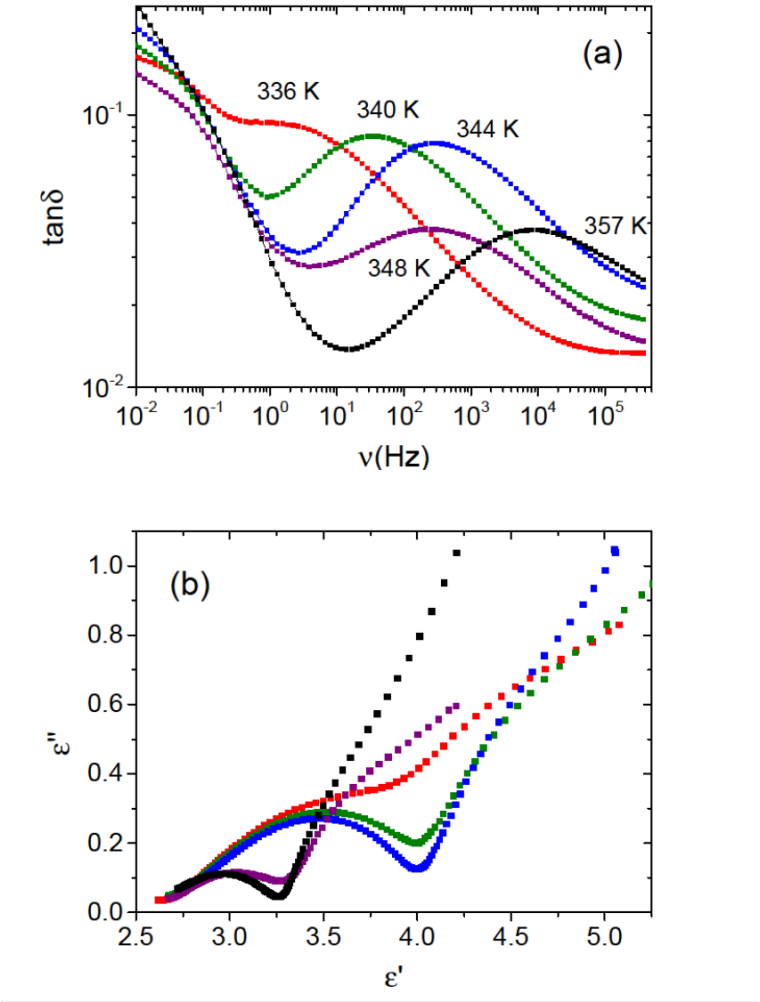

Figure 5. Tan(δ) vs. frequency (a) and Cole-Cole plots (b) for the segmental mode of PLLA/f-CNT0.5/R. The spectra are shown at selected temperature in the temperature range between 336 and 357 K, where the segmental mode (α relaxation) is observed.

The variation of tan(δ) with temperature of the PLLA/f-CNT0.5/R sample is shown in Figure 6 for two different fixed frequencies (1.3 Hz and 1.3 kHz). As expected, both the segmental (α) relaxation (visible above room temperature) and the *β* relaxation (visible below 0 ºC) shift to higher temperature with increasing frequency. At the frequency of 1.3 kHz, as the temperature is raised through the crystallization temperature ($T_c \approx 340$ K), the value of ε" undergoes a

sudden drop, more clearly visible in the inset to Figure 6. This is obviously due to the reduction in strength of the α relaxation when partial crystallization takes place intensity.

At the fixed frequency of 1.3 Hz, the change at 340 K is not as visible, since at the crystallization temperature this frequency is well on the low-frequency side of the α loss peak. The drop visible at the fixed frequency of 0.01 Hz in the inset to Figure 6 is instead due to the reduction of conductivity when partial crystallization takes place. The tan(δ) values at 1.3 Hz after crystallization were higher in the samples with CNTs than without them (see Figure 8(a)), in agreement with the expectation that heterogeneity effects are more pronounced in the presence of the nanofillers, and in line with the increase in intensity of the interfacial (MWS) relaxation in these samples compared with chain-extended PLLA.

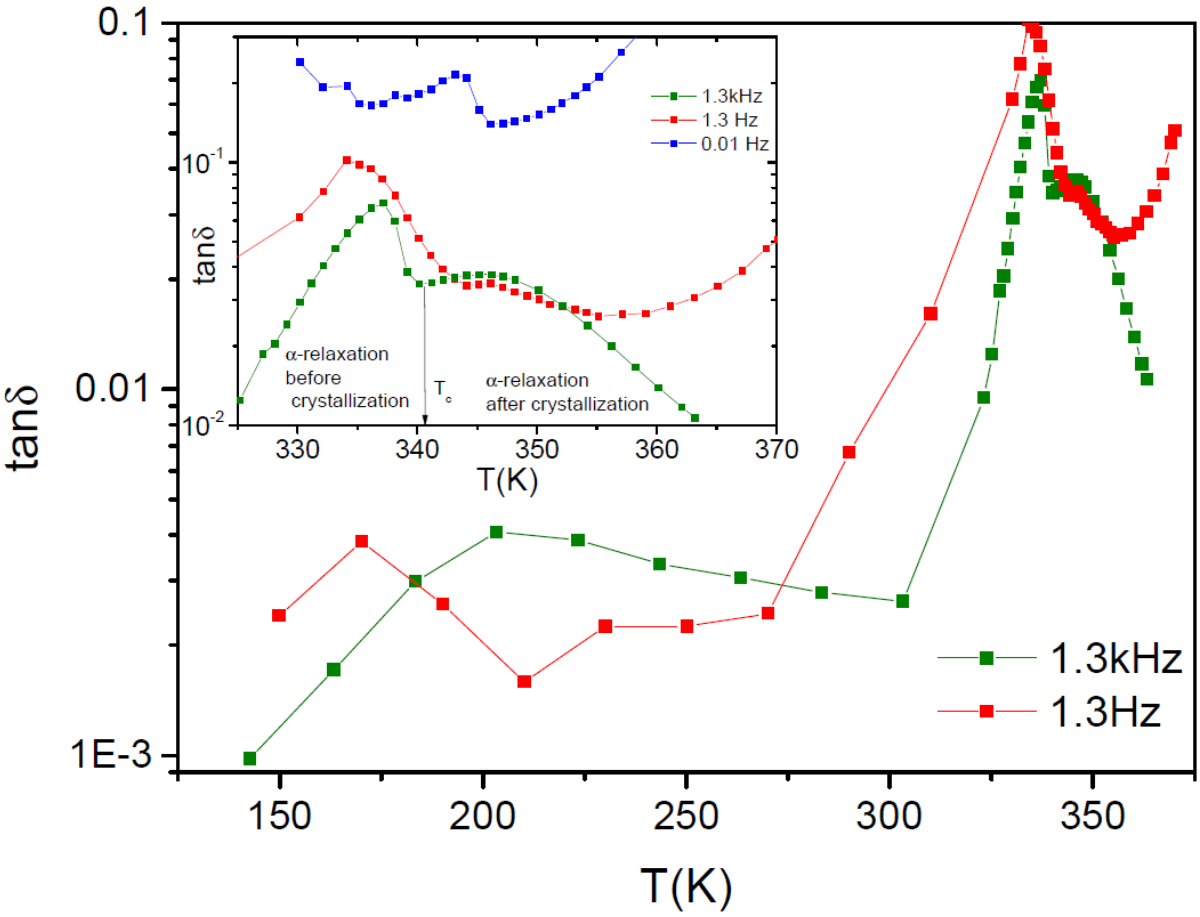

Figure 6. Tan(δ) *vs* temperature at different frequencies for the PLLA/f-CNT0.5/R. Inset: zoom-in in the temperature interval above T_g, where partial crystallization takes place (T_c).

The Arrhenius plots of the α relaxation time (τ) and dielectric strength ($\Delta\varepsilon$) for pure PLLA and for the nanocomposites are shown in figure 7. Both $\Delta\varepsilon$ and τ display a discontinuity corresponding to the (partial) crystallization of the polymer, which takes place at slightly different temperatures in the various samples. Before crystallization, the dielectric strength has a slightly increasing trend (Figure 7(b)).

It is observed in Figure 7(a) that τ is almost independent of MWCNT content, both before and after partial crystallization takes place. Close to T_g, that is, prior to partial crystallization, the Arrhenius plot of the α relaxation time exhibits a clear curvature, *i.e.*, a non-Arrhenius

behavior. After partial crystallization of the polymer the curvature of the cooperative segmental relaxation is less obvious, but it is still present as visible in the τ values acquired in a series of spectra acquired on the partially crystalline samples at lower temperature (open markers in Figure 7(a). The curvature of the Arrhenius plot is related to the so-called kinetic fragility of the glass former [38, 39] as described below. The absolute value of the relaxation time is lower just after crystallization than at its onset, which can be rationalized considering that the crystallization of a (or a part of) polymer chain hinders the motion of the rest of the chain and of neighboring chains. Measurements carried out cooling down the partially crystallized samples (performed shortly after partial crystallization took place) indicate that, when characterized in a wider temperature interval, the amorphous fraction in the partially crystallized sample actually follows a sub-Arrhenius curve, with a significantly different T_g value compared with the fully amorphous polymer samples.

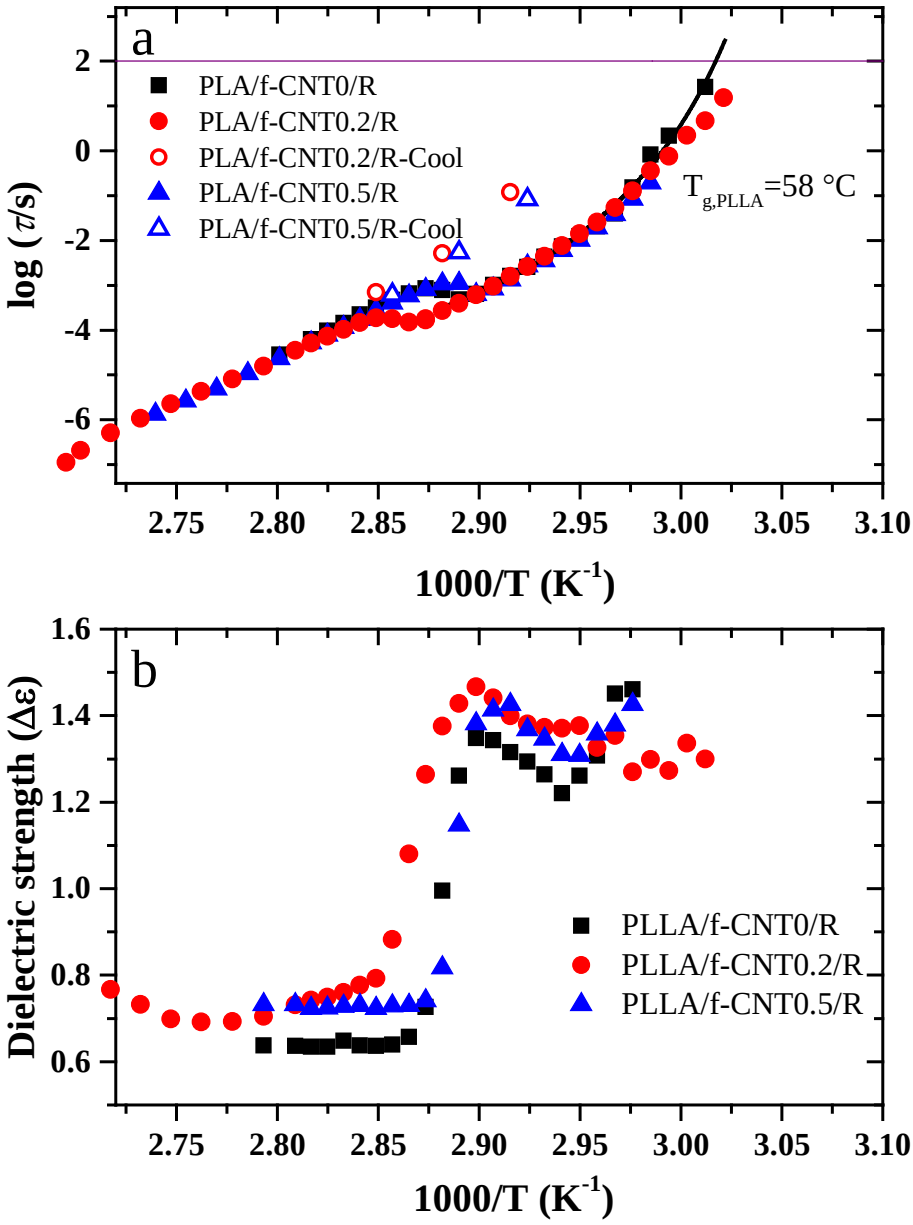

Figure 7. Arrhenius plot of the relaxation time (a) and dielectric strength (b) of the cooperative segmental relaxation (α) at different temperatures for PLLA and the nanocomposites with 0.2 and 0.5 wt-% CNT.

A wide variety of models have been proposed to describe the non-Arrhenius temperature dependence of relaxation time and viscosity of supercooled liquids. The extensive discussion of

applicability of these formulas is presented in references [40, 41]. The most frequently used equation is the empirical Vogel–Fulcher–Tammann (VFT) law [42]:

$$\log \tau = \log \tau_{\infty} + \frac{1}{ln10} \frac{DT_0}{T - T_0} \tag{9}$$

Here, τ_{∞} is the high temperature limit of the relaxation time, T_0 is the Vogel-Fulcher temperature, and D is the so-called "strength parameter", related to the kinetic fragility of the system. From the VFT equation a convenient measure for the fragility (m) can be defined in terms of the effective activation energy at T_g:

$$m = \left. \frac{d \log \tau}{d(T_g / T)} \right|_{T = T_g} = \frac{DT_0 T_g}{2.303(T_g - T_0)^2} \tag{10}$$

The values of τ_{∞}, D and T_0 obtained by fitting the experimental data close to T_g (prior to crystallization) to equation 9 are presented in Table 2. Higher values of D indicate stronger (less fragile) glass formers [39]. From the results of Table 2, it is seen that the sample PLLA/f-CNT0.2/R showed the highest D value (lowest m value) compared to other samples. The lower fragility value for the sample PLLA/f-CNT0.2/R might be related to the better dispersion state of CNT and bonding of PLLA and carboxylated CNTs, as discussed in our previous work [12, 27]. The dielectric T_g values are higher by roughly 3 K before and after crystallization (not shown), which is consistent with the variation of the calorimetric T_g upon partial crystallization reported in Table 1 (of the order of 1.5 or 2 K).

Table 2. Vogel-Fulcher parameters, fragility and dielectric glass transition temperatures (prior to partial crystallization) for the segmental mode of chain-extended PLLA and the nanocomposites with 0.2 and 0.5 wt-% carboxylated CNT.

Sample	log (τ_∞/[s])	T_0 [K]	D	m	T_g [K]
PLLA/f-CNT0/R	-7.2±0.5	314±1	0.71±0.12	120±20	331±1
PLLA/f-CNT0.2/R	-9.2±0.9	313±4	1.4±0.5	94±10	330±1
PLLA/f-CNT0.5/R	-8±1	315±3	1.1±0.3	100±30	330±3

Figure 8(a) shows the tan(δ) value at 1.3 Hz as a function of temperature, both for pure PLLA and for the two nanocomposites. All samples displayed a maximum of tan(δ) around 58 °C; however, addition of f-CNT during the chain extension reaction resulted in different values of tan(δ). A constrained interfacial layer of polymer is formed close to each nanotube, and the establishment of multiple polymer-nanoparticle interactions influences the glassy behavior and transition of the polymer chains [3]. These constrained polymer chains (schematically shown in the inset to Figure 8a) are the immobilized polymer segments anchored to the nanotube surfaces, and neighboring chains that become stiffer due to their proximity to the immobilized segments. As discussed in our previous work on dynamic mechanical analysis (DMA) [3, 27], for amorphous polymers the constrained volume fraction (φ) of PLLA chains around nanoparticles can be estimated by the tan(δ) value at the glass transition temperature. The use of tan(δ) for this purpose is justified by the fact that, while ε" is an extensive quantity, tan(δ) is an intensive one, hence it does not depend on the mass fraction of polymer in the samples. The constrained (interfacial) polymer region does not dissipate energy, and its fraction may be expressed in terms of the ratio between the energy loss of the composite (E) and the neat polymer (E_0) as [43]:

$$\varphi = 1 - \frac{E}{E_0} \tag{11}$$

where

$$E = \frac{\pi \tan \delta}{\pi \tan \delta + 1} \tag{12}$$

With the so-obtained values of φ, the thickness of interphase (t_i) can be found by the following equation [27]:

$$\frac{\varphi}{\varphi_{np}} = \frac{4}{3}\left(\frac{4t_i^3 + 3t_i^2}{D^2 L}\right) + \frac{2(\pi t_i^2 + D t_i + 2L t_i)}{DL} + 1 \tag{13}$$

where φ_{np} is the volume fraction of nanofiller in the system and D and L are the typical diameter and length of the nanotubes, respectively.

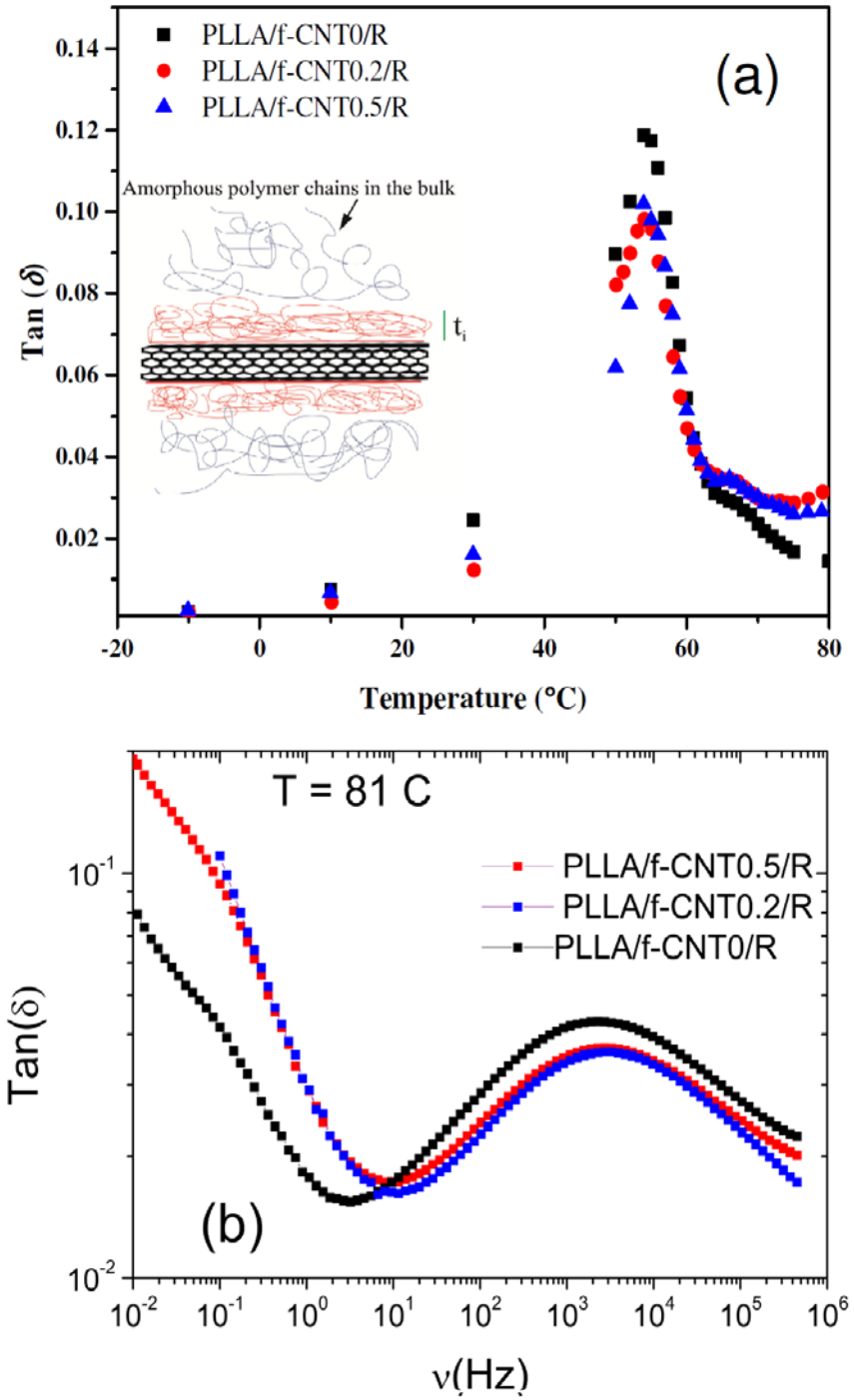

Figure 8. (a) Tan(δ) *versus* temperature for PLLA and the nanocomposites, at the frequency of 1.3 Hz. A schematic of amorphous polymer chains in the bulk (blue lines) and at the interphase (red lines) is presented at inset. (b) Tan(δ) *versus* frequency for all samples at 354 K.

The results for the constrained volume fraction and thickness of interphase obtained by means of these equations are presented in Table 3. Compared to the PLLA/f-CNT0.5/R sample, the sample with 0.2wt-% of CNT showed more constrained polymers and higher interphase values due to better dispersion state and more extensive bonding between PLLA and CNT. As discussed in our previous work [12, 27], during the chain extension reaction the carboxylated CNTs can participate in the reaction and consume the epoxied chain extender. Since the chain extender is multifunctional epoxy, for a relatively low amount of f-CNT (i.e. 0.2 wt-%) the formation of bonds between PLLA and f-CNT is more probable, and the dispersion state of f-CNT is improved in this case.

Table 3. Constrained volume fraction (φ) of amorphous PLLA chains and thickness of the interphase layer.

Sample	E^a	φ^a *(vol.%)*	φ^b *(vol.%)*	t_i^a *(nm)*	t_i^b *(nm)*
PLLA/f-CNT0/R	0.272	-	-	-	-
PLLA/f-CNT0.2/R	0.235	13.6	3.5	46	21
PLLA/f-CNT0.5/R	0.243	10.9	2.8	24	12

[a]Results by BDS (this work)
[b]Results by DMA (ref. [27])

The DMA results on the constrained amorphous fraction [27] showed the same trend as the BDS study presented here. It is interesting to note that the values of constrained polymer chains obtained by BDS are significantly higher than those of DMA. The difference in the two

measurements is tentatively assigned to the different measuring principle of both techniques. Because BDS experiment detects changes in the orientational polarization due to permanent dipole moments, while DMA is sensitive to mechanical deformation, the “rigidity” of the interfacial layer is actually defined, in the BDS case, by the lack of motion of dipolar subunits, whose motion may or may not be directly coupled with those that are responsible for a given mechanical response [1].

As mentioned earlier, the “tail” to the right of the semicircle in the Cole-Cole plot corresponds to the MWS relaxation observed at low frequency in the loss spectra, which is related to the heterogeneity of the sample. It is obvious from Figure 9 that the three studied samples have different heterogeneity (different tails) in the amorphous and partially crystalline state. Here we extend a newly introduced criterion [12] to compare the heterogeneity of different samples at 333 K and 347 K, namely the start-to-end length of the tail as indicated by dotted lines in Figure 8, which we define as the heterogeneity (*H*) index. The calculated *H* indices are presented in Table 4 at 333 K and 347 K. It is expected that addition of CNTs in the PLLA should increase the heterogeneity of the system due to the creation of new interfaces, and the different behavior of the bulk polymer compared with the polymer at the nanotube surface. According to the results of Table 4, the heterogeneity of sample with 0.5 wt-% is indeed highest compared to the other samples (at both temperatures). Hence our phenomenological introduction of the heterogeneity index is in line with expectations and with the DMA results. Note that this heterogenity arises from the difference between the dynamics of different polymer molecules. This deviation can be related to molecular weight distribution, chain structure and nanoparticles, a feature that needs to be studied further.

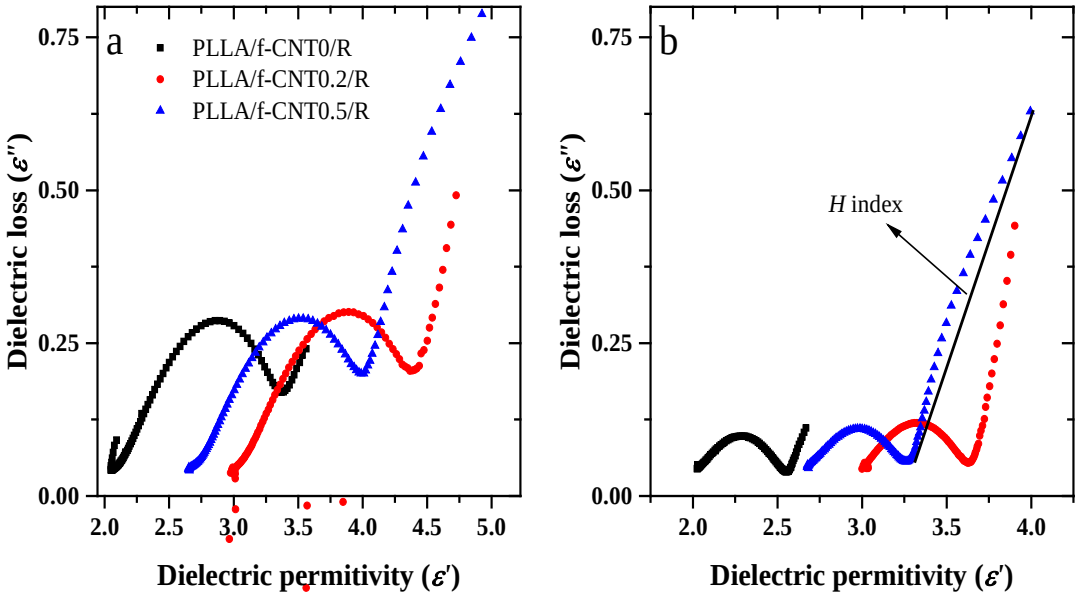

Figure 9. Cole-Cole plots at 333 K (a) and 347 K (b) in the frequency range of 0.1 Hz and 10^6 Hz for pure PLLA and the nanocomposites with 0.2 and 0.5 wt-% CNT. The length of the dotted segments is defined as heterogeneity (*H*) index.

Table 4. Calculated *H* index at two temperatures (333 and 347 K).

sample	*T* (K)	*H*
PLLA/f-CNT0/R	333	0.18
	347	0.34
PLLA/f-CNT0.2/R	333	0.38
	347	0.47
PLLA/f-CNT0.5/R	333	1.08
	347	1.21

CONCLUSIONS

The size of cooperative rearranging region (CRR), thermodynamic properties and molecular relaxation dynamics of nanocomposites based on chain-extended PLLA and carboxylated multi-wall carbon nanotubes (MWCNT) were investigated by temperature-modulated differential scanning calorimetry and broadband dielectric spectroscopy. The presence of the MWCNT barely affected the glass transition temperature (T_g) and the size of CRRs of the amorphous fraction. Both the pure chain-extended PLLA and the nanocomposites underwent partial crystallization upon heating above T_g. All samples display a smaller size of the CRR after partial crystallization, which indicates that the characteristic size of cooperativity is smaller, likely due to the constraints imposed by the presence of the rigid crystalline fraction. The cooperative segmental relaxation of the polymer became slower after partial crystallization, as expected due to the formation of rigid spherulites right next to the more mobile amorphous fraction. The tan(δ) values and the estimated rigid amorphous fraction of PLLA changed with addition of carboxylated MWCNTs. Both the constrained volume fraction φ and the thickness of interphase t_i, as determined from BDS experiments, are higher in the nanocomposites, in agreement with previous DMA results, confirming the existence of strong interactions between PLLA and MWCNT. The interphase thickness is higher in the sample with 0.2 wt-% f-CNT. A new criterion was identified to quantify the (dynamical) heterogeneity of polymeric samples, based on the low-frequency arc in Cole-Cole plots. Lower heterogeneity was observed for PLLA/f-CNT0.2/R sample, due to the lower MWCNT content and possibly also to a better dispersion state in this sample.

ACKNOWLEDGEMENTS

J.P., R.M. and S.V. are grateful to acknowledge support from the Spanish Ministry of Economy and Competitiveness MINECO and FEDER (projects MAT2015-69547-R and FIS2017-82625-P). R.M. and J.P. acknowledge support by the Generalitat de Catalunya under projects 2017SGR-42 and 2017SGR-373, respectively.

REFERENCES

[1] Y. Rao, J.M. Pochan, Mechanics of Polymer−Clay Nanocomposites, Macromolecules, 40 (2007) 290-296.
[2] O. Yousefzade, F. Hemmati, H. Garmabi, M. Mahdavi, Thermal behavior and electrical conductivity of ethylene vinyl acetate copolymer/expanded graphite nanocomposites: Effects of nanofiller size and loading, Journal of Vinyl and Additive Technology, 22 (2016) 51-60.
[3] O. Yousefzade, H. Garmabi, Development of a simple model to characterize the complex constrained polymer chains in polymer nanocomposites at the interphase of amorphous/semicrystalline ethylene vinyl acetate and nanosheets, Journal of Composite Materials, 51 (2017) 179-186.
[4] J. Ren, O. Urakawa, K. Adachi, Dielectric and Viscoelastic Studies of Segmental and Normal Mode Relaxations in Undiluted Poly(d,l-lactic acid), Macromolecules, 36 (2003) 210-219.
[5] J. Ren, O. Urakawa, K. Adachi, Dielectric study on dynamics and conformation of poly(d,l-lactic acid) in dilute and semi-dilute solutions, Polymer, 44 (2003) 847-855.
[6] J.F. Mano, J.L. Gómez Ribelles, N.M. Alves, M. Salmerón Sanchez, Glass transition dynamics and structural relaxation of PLLA studied by DSC: Influence of crystallinity, Polymer, 46 (2005) 8258-8265.
[7] B. Rijal, L. Delbreilh, A. Saiter, Dynamic Heterogeneity and Cooperative Length Scale at Dynamic Glass Transition in Glass Forming Liquids, Macromolecules, 48 (2015) 8219-8231.
[8] G. Adam, J.H. Gibbs, On the Temperature Dependence of Cooperative Relaxation Properties in Glass-Forming Liquids, The Journal of Chemical Physics, 43 (1965) 139-146.
[9] E. Hempel, G. Hempel, A. Hensel, C. Schick, E. Donth, Characteristic Length of Dynamic Glass Transition near Tg for a Wide Assortment of Glass-Forming Substances, The Journal of Physical Chemistry B, 104 (2000) 2460-2466.
[10] E. Donth, The size of cooperatively rearranging regions at the glass transition, Journal of Non-Crystalline Solids, 53 (1982) 325-330.
[11] D. E., Characteristic length of the glass transition, Journal of Polymer Science Part B: Polymer Physics, 34 (1996) 2881-2892.
[12] O. Yousefzade, H. Garmabi, J. Puiggali, Cooperative rearranging region and dynamical heterogeneity of nanocomposites in poly(l-lactide) and functionalized carbon nanotubes systems, Thermochimica Acta, 667 (2018) 35-41.
[13] N. Delpouve, A. Saiter, J.F. Mano, E. Dargent, Cooperative rearranging region size in semi-crystalline poly(l-lactic acid), Polymer, 49 (2008) 3130-3135.
[14] O. Yousefzade, J. Jeddi, E. Vazirinasab, H. Garmabi, Poly(lactic acid) phase transitions in the presence of nano calcium carbonate:Opposing effect of nanofiller on static and dynamic measurements, Journal of Thermoplastic Composite Materials, 0 0892705718759386.
[15] M. Karevan, K. Kalaitzidou, Formation of a complex constrained region at the graphite nanoplatelets-polyamide 12 interface, Polymer, 54 (2013) 3691-3698.

[16] P. Klonos, S. Kripotou, A. Kyritsis, G.Z. Papageorgiou, D. Bikiaris, D. Gournis, P. Pissis, Glass transition and segmental dynamics in poly(l-lactic acid)/graphene oxide nanocomposites, Thermochimica Acta, 617 (2015) 44-53.
[17] Y. Feng, O. Yuchun, Y. Zhongzhen, Polyamide 6/silica nanocomposites prepared by in situ polymerization, Journal of Applied Polymer Science, 69 (1998) 355-361.
[18] D. Fragiadakis, P. Pissis, L. Bokobza, Glass transition and molecular dynamics in poly(dimethylsiloxane)/silica nanocomposites, Polymer, 46 (2005) 6001-6008.
[19] S. Gong, Q. Chen, J.F. Moll, S.K. Kumar, R.H. Colby, Segmental Dynamics of Polymer Melts with Spherical Nanoparticles, ACS Macro Letters, 3 (2014) 773-777.
[20] G. Tsagaropoulos, A. Eisenberg, Dynamic Mechanical Study of the Factors Affecting the Two Glass Transition Behavior of Filled Polymers. Similarities and Differences with Random Ionomers, Macromolecules, 28 (1995) 6067-6077.
[21] A. Sargsyan, A. Tonoyan, S. Davtyan, C. Schick, The amount of immobilized polymer in PMMA SiO2 nanocomposites determined from calorimetric data, European Polymer Journal, 43 (2007) 3113-3127.
[22] Y. Lin, L. Liu, G. Xu, D. Zhang, A. Guan, G. Wu, Interfacial Interactions and Segmental Dynamics of Poly(vinyl acetate)/Silica Nanocomposites, The Journal of Physical Chemistry C, 119 (2015) 12956-12966.
[23] P. Klonos, Z. Terzopoulou, S. Koutsoumpis, S. Zidropoulos, S. Kripotou, G.Z. Papageorgiou, D.N. Bikiaris, A. Kyritsis, P. Pissis, Rigid amorphous fraction and segmental dynamics in nanocomposites based on poly(l–lactic acid) and nano-inclusions of 1–3D geometry studied by thermal and dielectric techniques, European Polymer Journal, 82 (2016) 16-34.
[24] S. Valenti, M. Romanini, L. Franco, J. Puiggalí, J.L. Tamarit, R. Macovez, Tuning the Kinetic Stability of the Amorphous Phase of the Chloramphenicol Antibiotic, Molecular Pharmaceutics, (2018) DOI: 10.1021/acs.molpharmaceut.8b00786.
[25] R.W. Sillars, The properties of a dielectric containing semiconducting particles of various shapes, in: Institution of Electrical Engineers - Proceedings of the Wireless Section of the Institution, 1937, 139-155.
[26] G. Perrier, A. Bergeret, Polystyrene–glass bead composites: Maxwell–Wagner–Sillars relaxations and percolation, Journal of Polymer Science Part B: Polymer Physics, 35 (1997) 1349-1359.
[27] O. Yousefzade, H. Garmabi, J. Puiggalí, M.H. Moghadam, Rigid amorphous phase and constrained polymer chains in poly(L-lactide) nanocomposites with carboxylated carbon nanotubes prepared via reactive melt mixing, Polymer Composites, 39 (2018) 1280-1293.
[28] E.W. Fischer, H.J. Sterzel, G. Wegner, Investigation of the structure of solution grown crystals of lactide copolymers by means of chemical reactions, Kolloid-Zeitschrift und Zeitschrift für Polymere, 251 (1973) 980-990.
[29] S. Havriliak, S. Negami, A complex plane representation of dielectric and mechanical relaxation processes in some polymers, Polymer, 8 (1967) 161-210.
[30] M. Avrami, Granulation, Phase Change, and Microstructure Kinetics of Phase Change. III, The Journal of Chemical Physics, 9 (1941) 177-184.
[31] M. Zachariah, M. Romanini, P. Tripathi, M. Barrio, J.L. Tamarit, R. Macovez, Self-Diffusion, Phase Behavior, and Li+ Ion Conduction in Succinonitrile-Based Plastic Cocrystals, The Journal of Physical Chemistry C, 119 (2015) 27298-27306.
[32] J. Ren, K. Adachi, Dielectric Relaxation in Blends of Amorphous Poly(dl-lactic acid) and Semicrystalline Poly(l-lactic acid), Macromolecules, 36 (2003) 5180-5186.
[33] E. Laredo, D. Newman, R. Pezzoli, A.J. Müller, A. Bello, A complete TSDC description of molecular mobilities in polylactide/starch blends from local to normal modes: Effect of composition, moisture, and crystallinity, Journal of Polymer Science Part B: Polymer Physics, 54 (2016) 680-691.
[34] P. Tripathi, M. Romanini, J.L. Tamarit, R. Macovez, Collective relaxation dynamics and crystallization kinetics of the amorphous Biclotymol antiseptic, International Journal of Pharmaceutics, 495 (2015) 420-427.

[35] G.N. Ruiz, M. Romanini, M. Barrio, J.L. Tamarit, L.C. Pardo, R. Macovez, Relaxation Dynamics vs Crystallization Kinetics in the Amorphous State: The Case of Stiripentol, Molecular Pharmaceutics, 14 (2017) 3636-3643.
[36] P.A.M. Steeman, J. van Turnhout, Fine Structure in the Parameters of Dielectric and Viscoelastic Relaxations, Macromolecules, 27 (1994) 5421-5427.
[37] M. Wübbenhorst, J. van Turnhout, Analysis of complex dielectric spectra. I. One-dimensional derivative techniques and three-dimensional modelling, Journal of Non-Crystalline Solids, 305 (2002) 40-49.
[38] C.A. Angell, Spectroscopy simulation and scattering, and the medium range order problem in glass, Journal of Non-Crystalline Solids, 73 (1985) 1-17.
[39] R. Böhmer, K.L. Ngai, C.A. Angell, D.J. Plazek, Nonexponential relaxations in strong and fragile glass formers, The Journal of Chemical Physics, 99 (1993) 4201-4209.
[40] F. Stickel, E.W. Fischer, R. Richert, Dynamics of glass-forming liquids. I. Temperature-derivative analysis of dielectric relaxation data, The Journal of Chemical Physics, 102 (1995) 6251-6257.
[41] F. Stickel, E.W. Fischer, R. Richert, Dynamics of glass-forming liquids. II. Detailed comparison of dielectric relaxation, dc-conductivity, and viscosity data, The Journal of Chemical Physics, 104 (1996) 2043-2055.
[42] F.G. S., Analysis of recent measurements of the viscosity of glasses, Journal of the American Ceramic Society, 8 (1925) 339-355.
[43] Y. Kojima, A. Usuki, M. Kawasumi, A. Okada, Y. Fukushima, T. Kurauchi, O. Kamigaito, Mechanical properties of nylon 6-clay hybrid, Journal of Materials Research, 8 (2011) 1185-1189.